Assessment of the Arsenic Removal From Water Using Lanthanum Ferrite

Fabiana E. García,[a] Marta I. Litter,[b] and Isabella Natali Sora*[c]

The catalytic performance of a perovskite-type lanthanum ferrite $LaFeO_3$ to remove arsenic from water has been investigates for the first time. $LaFeO_3$ was prepared by citrate auto-combustion of dry gel obtained from a solution of the corresponding nitrates poured into citric acid solution. Kinetic studies were performed in the dark with As(V) and in the dark and under UV-C irradiation at pH 6–7 with As(III) (both 1 mg L^{-1}), and As:Fe molar ratios (MR) of 1:10 and 1:100 using the $LaFeO_3$ catalyst. As(V) was removed from solution after 60 min in the dark in 7% and in 47% for MR = 1:10 and MR = 1:100, respectively, indicating the importance of the amount of the iron material on the removal. Oxidation of As(III) in the dark was negligible after 60 min in contact with the solid sample, but complete removal of As(III) was observed within 60 min of irradiation at 254 nm, due to As(III) photooxidation to As(V) and to As(III) sorption to a minor extent. Morphological and microstructural studies of the catalyst complement the catalytic testing. This work demonstrates that $LaFeO_3$ can be used for the removal of As(III) from highly arsenic contaminated water.

1. Introduction

Arsenic contamination in drinking water is a serious concern in many countries, in particular those in South and South-East Asia and in Latin America. Overexposure to As and its compounds is known to have a hazardous effect on the human health.[1] Thus, the World Health Organization (WHO) recommends 10 μg L^{-1} as the maximum allowed amount for As in water for human consumption. The presence of As is the result of several processes, especially natural and anthropogenic in a minor extent. Natural processes are mainly geogenic, such as the dissolution in water of arsenic-containing rocks and, among anthropogenic processes, the discharge of effluents containing industrial and mining wastes. Arsenic occurs both in inorganic and organic forms in natural waters, but inorganic As is the most commonly chemical form found. Inorganic As exists in two oxidation states, As(III) or As(V), depending on oxygen concentration, Eh and pH of the solution. In oxygenated water (for example surface waters), As is mainly present as arsenate (As(V)) and, under anoxic reducing conditions (in groundwater aquifers), as arsenite (As(III)). However, due to slow redox reactions, As(III) and As(V) are present in both environments.[2]

Arsenic removal from water can be achieved through oxidation, coagulation-flocculation and membrane processes,[3] among other technologies. Generally, the process consists of several steps: firstly, the oxidation of soluble As(III) (if present) to As(V) occurs and then, at the same time or sequentially, coagulant agents (for example iron coagulants) are used followed by adsorption or membrane\filtration.[4] This strategy shows two main drawbacks, such as a certain low adsorption capacity of the sorbent materials (iron, aluminum or titanium oxides), and the complex regeneration/disposal of the As-sorbent. Cation-exchange resins can provide a one-step process, but they need stringent operating conditions for pH and water matrices.

Among the many processes that are used to oxidize As(III) in water, those based on heterogeneous photocatalysis have been widely studied. The exploitation of titanium dioxide (TiO_2) as photocatalyst and UV light is proved particularly effective due to the good chemical and environmental stability of TiO_2 and the strong oxidizing power of the holes generated in the photocatalyst under irradiation.[5–7] Moreover, TiO_2 is capable to adsorb As(V) from water in the dark.[8] However, in water treatment plants, the application of the photocatalytic oxidation using TiO_2 is uncommon, limited by the fact that the regeneration of TiO_2 loaded with the adsorbed As is difficult to achieve.[5] In addition, titania can only absorb UV light, which is only 3–5% of solar light due to its large bandgap of 3.0 eV above, which limits its applications.[9]

Among the photocatalysts, lanthanum ferrite ($LaFeO_3$), a perovskite-type ferrite, has gained considerable interest due to its easy synthesis, combined with remarkable performance

[a] Dr. F. E. García
División Química de la Remediación Ambiental
Gerencia Química, CAC, CNEA, CONICET
Av. Gral. Paz 1499
1650, San Martín, Prov. de Buenos Aires (Argentina)
[b] Prof. M. I. Litter
IIIA (CONICET-UNSAM)
Universidad Nacional de General San Martín
Campus Miguelete
Av. 25 de Mayo y Francia
1650 San Martín, Prov. de Buenos Aires (Argentina)
[c] Prof. I. N. Sora
INSTM R.U. and Department of Engineering and Applied Sciences
University of Bergamo
viale Marconi 5
24044 Dalmine (BG), (Italy)
E-mail: isabella.natali-sora@unibg.it

Supporting information for this article is available on the WWW under https://doi.org/10.1002/open.202100065

stability, low-cost, non-toxicity and natural abundance.[10] Several applications like electrodes,[11] chemical sensors,[12] and catalysts[13–14] have been explored for $LaFeO_3$.[10,15–17] Perovskite ferrites are subclasses of iron oxides with general formula ABO_3 and show the crystal structure of the archetypical perovskite $CaTiO_3$.[18] Most of the ferrite perovskites have their native bandgaps in the visible region. Use of hematite and other iron oxide compounds have known shortcomings for their use as photocatalysts such as short exciton diffusion length, low electron conductivity, and lower conduction band edge potential. However, certain ferrite-based perovskites have shown good photocatalytic activities, circumventing the shortcomings seen in binary iron oxides.

$LaFeO_3$ possesses a relatively narrow bandgap energy of around 2.5 eV.[14] It has been proposed as visible-light and UV photocatalyst for aqueous reactions,[19–23] often combined with a Fenton-like reaction.[24–25] It has been explored for degradation of pollutants as well as for hydrogen evolution under visible light.[26]

$LaFeO_3$, as many perovskite-type oxides, shows a high recombination rate of photogenerated electron-hole (e^--h^+) pairs.[27] Several strategies are developed to reduce the unfavorable electron-hole recombination process such as doping with transition metal elements,[28–29] fabrication of composites,[30–31] and decoration with Ag.[32] However, these solutions show inherent drawbacks such as a lower chemical stability with respect to the pure $LaFeO_3$, and complexity of fabrication. For these reasons, we plan to use pure $LaFeO_3$ for photocatalytic tests in water. Furthermore, $LaFeO_3$ is a p-type semiconductor. By definition, p-type semiconductors have a larger concentration of holes than electron concentration. In p-type semiconductors, holes are the majority carriers and electrons are the minority carriers. This is excellent to improve oxidation reactions.

Generally, the studies on photocatalysis with $LaFeO_3$ have been made using degradation of dyes.[10,15,17] For the first time, the use of $LaFeO_3$ as effective photocatalyst for As(III) oxidation to As(V) from water under UV-C irradiation is reported, with the purpose of exploring an alternative photocatalyst to TiO_2. UV-C radiation is a known disinfectant for water, which has been used for decades to reduce the spread of bacteria. The use of UV-C light to irradiate $LaFeO_3$ can remove the arsenic from water and, at the same time, can disinfect the water.

The catalyst is subjected to X-ray powder diffraction (XRD), Diffuse Reflectance UV-Vis (DRS) and Fourier Transform-infrared (FT-IR) spectroscopies to determine the microstructural properties. The catalyst starting and recovered after the removal tests was analyzed by Scanning electron microscopy (SEM) equipped with an energy-dispersive X-ray spectroscopy analyzer (EDS) detector to study microstructural modification formed during reaction.

2. Results and Discussion

2.1. Catalyst Characterization

The XRD pattern of powder $LaFeO_3$ is illustrated in Figure 1. The pattern displays peaks that are consistent with an orthorhombic perovskite, with some degree of broadening resulting from the nanocrystalline nature of the powder. The experimental data shows a very close match with the JCPDS (file: 00-037-1493) pattern, indicating phase purity. The size of the crystallites was 43 nm, calculated by using the Scherrer formula. The SSA of the sample was 13 $m^2 g^{-1}$, in agreement with Refs. [10, 14, 15, 17]. The surface structure of the $LaFeO_3$ powder was investigated by FT-IR spectroscopy. Figure 1 shows the FT-IR spectrum of the $LaFeO_3$ powder from 4000 to 600 cm^{-1}. The spectrum exhibits a broad band between about 3700 and 2800 cm^{-1} primarily caused by O–H stretching vibrations from water molecules. The O–H bending mode results in an absorption band at 1635 cm^{-1}. The additional bands at about 1491–1478 and 1386 cm^{-1} can indicate adsorbed carbonate groups on the particle surface. In particular, the value of the splitting of the ν3 vibration (due to asymmetric CO stretching) is about 100 cm^{-1}, which indicates the presence of monodentate metal carbonates. The carbonate groups can be due to CO_2 reactive adsorption (reaction products) on the surface of the perovskite as a result of the

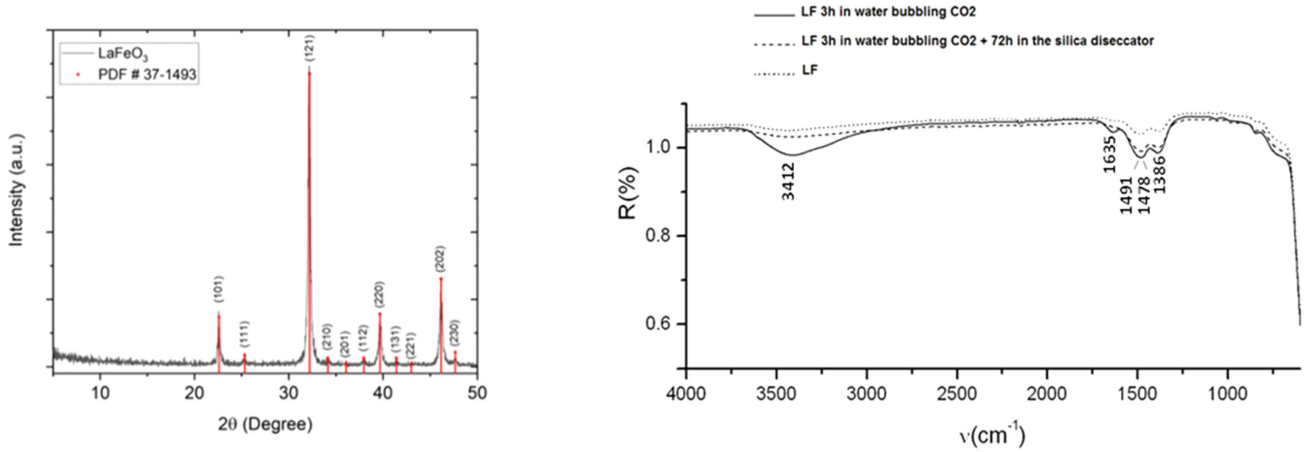

Figure 1. Left: XRD pattern of fresh powder $LaFeO_3$. The match with the reference pattern JCPDS file 00-037-1493 (red bars) is very high. Right: FT-IR spectra obtained at room temperature for the $LaFeO_3$ sample under different conditions shown in the legends.

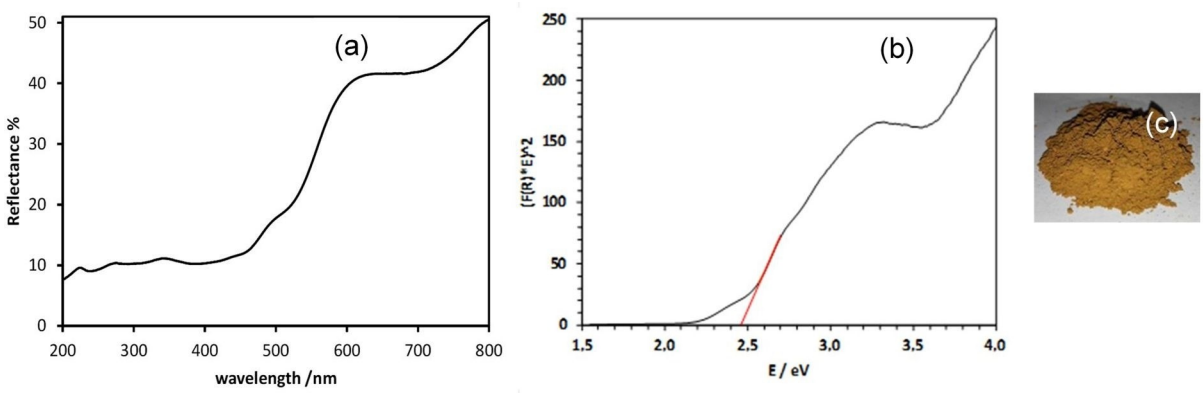

Figure 2. (a) DRS spectrum of fresh $LaFeO_3$ powder. (b) Plot of Kubelka-Munk function $(F(R_\infty)*E)^2$ vs. E obtained from DRS for band gap calculation. (c) Photographic image of the $LaFeO_3$ powder.

exposure to ambient air, and to a minor amount to remnants of citric acid. For comparison purposes, we also investigated the effect of the soaking the $LaFeO_3$ powder in CO_2-rich water (3 h in water bubbling CO_2) followed by 72 h in a desiccator with silica. The treatment alters the FT-IR response; in fact, the bands at 1386, 1478 and 1491 cm^{-1} are stronger than those in the starting spectrum. As expected, the bands of the $LaFeO_3$ desiccated powder show an intermediate intensity between the treated and the starting sample. The typical Fe–O stretching vibration band and the peaks corresponding to Fe–O–Fe bending modes cannot be seen because they appear below 600 cm.[16]

The diffuse reflectance spectrum of $LaFeO_3$ powder was measured by DRS, and the plot in Figure 2 was obtained by analyzing this DRS spectrum using the Kubelka-Munk function $F(R_\infty)$.[36] The linear regression fit of the plot $(F(R_\infty)*E)^2$ vs. E (E indicates the energy of incident photons) suggests a direct bandgap transition of 2.48 eV, slightly less than that reported in Ref. [14] (2.56 eV). The small difference can be explained considering that the band-gap energy depends not only on the material, but also on characteristics like crystallinity, particle size and stoichiometry.

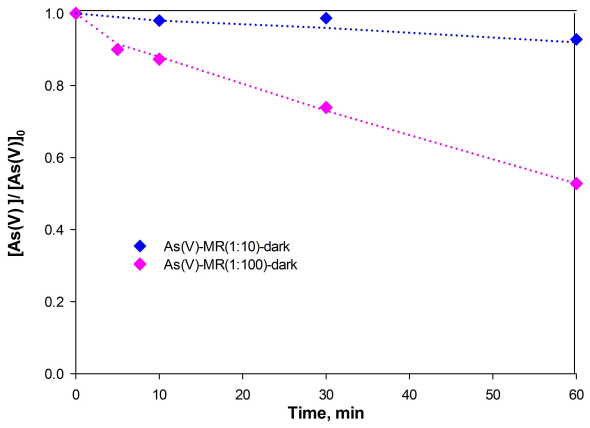

Figure 3. Evolution of the normalized As(V) concentration during the treatment of As(V) suspensions containing $LaFeO_3$ in the dark. Conditions: $As(V)]_0 = 1\ mg\,L^{-1}$, reaction volume V = 200 mL, MR = 1:10 and 1:100, t = 60 min, pH 7. The dotted lines are only for visualization and do not correspond to any fitting procedure.

2.2. Dark Reaction of As(V) Over $LaFeO_3$

Figure 3 shows experiments of As(V) removal in the presence of LaFeO3 in the dark with the reactor open to air. The conditions were:$As(V)]_0 = 1\ mg\,L^{-1}$, reaction volume V = 200 mL, MR = 1:10 and 1:100, t = 60 min, pH 7, T = 25 °C. As(V) was measured with the arsenomolybdate technique as indicated in the Experimental section. According to Figure 3, As(V) was removed from solution after 60 min in 7% and in 47% for MR = 1:10 and MR = 1:100, respectively, indicating the importance of the amount of the iron material on the removal of As(V) in the dark, surely due to an increased adsorption.

2.3. Dark and UV-C Irradiation of As(III) Over $LaFeO_3$

In Figure 4, results of As(III) ($1\ mg\,L^{-1}$) removal in the dark and under 254 nm irradiation in the presence of $LaFeO_3$ at two MR (1:30 and 1:100) are presented. The arsenomolybdate technique was used for As(III) measurement as indicated in the Experimental section. Figure 4 shows that As(III) removal in the dark at both MR is rather low. This is expected because the predominance of the neutral form of As(III) (H_3AsO_3) at the working pH,[3] which inhibits its adsorption on $LaFeO_3$. On the other hand, complete As(III) removal took place after 60 min under 254 nm irradiation at both MR. Additionally, it can be seen that As(III) removal increased with the increase of MR at the beginning of the reaction, but no large differences were observed with both MR at longer times (60 min). It's worth to note that a contribution caused by leached iron should be excluded, since in the range pH = 5–7 the solubility of $LaFeO_3$ is very low, less than $1\times10^{-3}\ mg\,L^{-1}$, as reported by Rusevova et al.[37]

Figure 5 shows the evolution of the normalized concentration of total As in solution (As_T) of the same experiments of Figure 4. Comparison of Figures 4 and 5 shows that the amount

of As_T in solution under irradiation is lower than the amount of As(III) removed under the same conditions, indicating that part of As remains adsorbed onto the photocatalyst surface, after being transformed to As(V) (see below). Irradiation under 254 nm increases As_T at both MR (1:30 and 1:100).

Figure 6 indicates the evolution of As(V) formation (MR (1:30 and 1:100)) in the dark and under 254 nm irradiation. There is almost no As(V) formation in the dark at any of both MR (note that the initial As(V) concentration is not null, probably due to As(III) oxidation during the manipulation of the samples). Under 254 nm irradiation, As(V) concentration increases with time. Formation of less As(V) at the highest MR is also observed, indicating that part of As(V) remains adsorbed on the surface of the material.

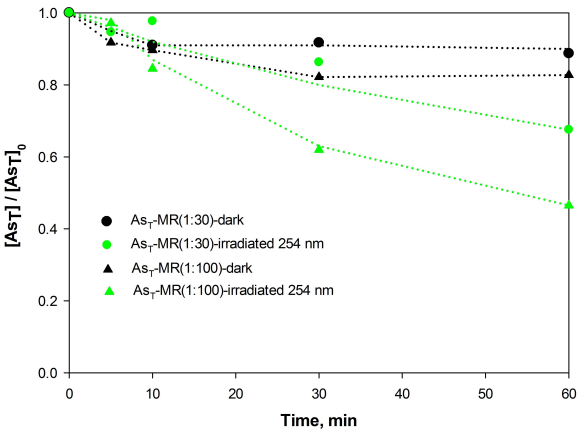

Figure 5. Evolution of the normalized As_T concentration during the treatment of As(III) suspensions containing $LaFeO_3$ in the dark and under 254 nm irradiation. Conditions of Figure 4. The dotted lines are only for visualization and do not correspond to any fitting procedure.

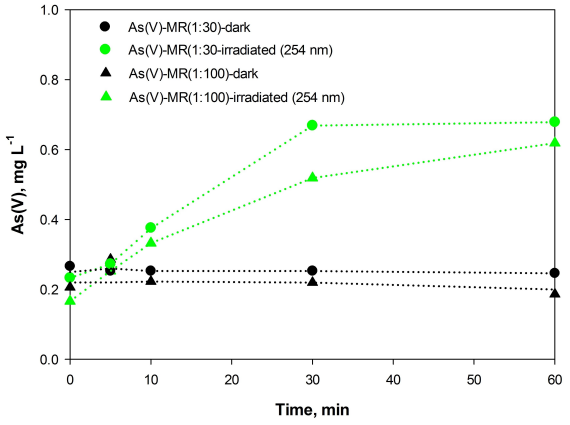

Figure 6. Evolution of the As(V) concentration during the treatment of As(III) suspensions containing $LaFeO_3$ in the dark and under 254 nm irradiation. Conditions of Figure 4. The dotted lines are only for visualization and do not correspond to any fitting procedure.

2.4. Catalyst Recovered After the Reaction of As

Figure 7(a) shows the SEM image of the starting $LaFeO_3$ powder, and Figures. 8 (a) and (a') illustrate the SEM images of the solids recovered after the irradiation of As(III) suspensions containing $LaFeO_3$ (MR = 1:100) at two different magnifications. SEM images of the starting $LaFeO_3$ powder showed clusters of particles in the range 100–400 μm and smaller aggregates below 10 μm. It is clearly seen that, after the arsenic removal tests, the $LaFeO_3$ samples have different morphology: the shape of the particles is less regular and the diameters of the $LaFeO_3$

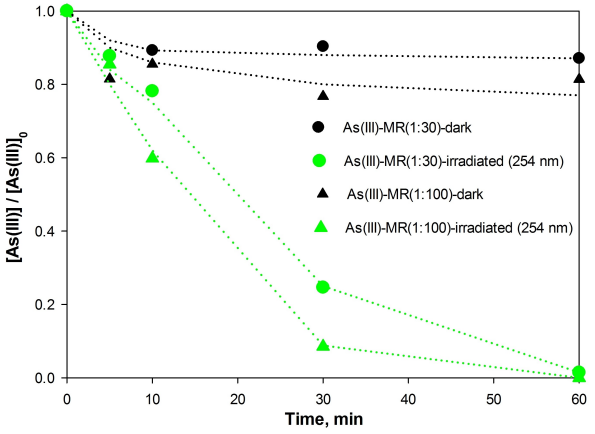

Figure 4. Evolution of the normalized As(III) concentration during the treatment of As(III) suspensions containing $LaFeO_3$ in the dark and under 254 nm irradiation. Conditions:$As(III)]_0 = 1$ mg L^{-1}, MR = 1:30 and 1:100, reactor open to air, pH 6–7, T = 25 °C. The dotted lines are only for visualization and do not correspond to any fitting procedure.

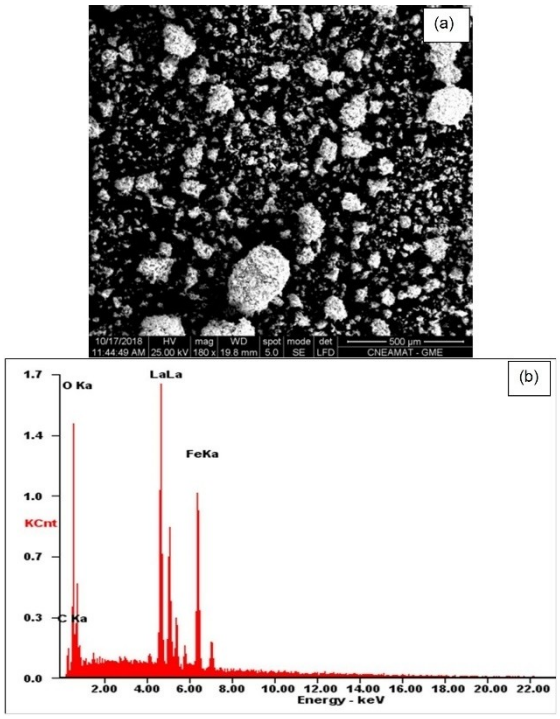

Figure 7. SEM image (a), and EDX analysis (b) of the $LaFeO_3$ powder before reaction with As.

aggregates are smaller (>20 μm) due to continuous stirring during the tests. In order to evaluate the compositional characteristics, EDX analysis was carried out on the samples.

Figure 7(b) shows the EDX spectrum of the starting $LaFeO_3$ powder, and Figure 8(b) illustrates the EDX spectrum of the solid obtained after the irradiation of As(III) suspensions containing $LaFeO_3$ (MR = 1:100). Signals from lanthanum, iron, carbon and oxygen were recorded. The normalized atomic ratio was both in the range La:Fe = 0.93–0.96:1 within the experimental error, slightly lower than the ratio reported by Parrino et al.[38] Moreover, the powder was always richer in oxygen than the nominal composition; this is not surprising and can be explained taking into account the presence of carbonate species detected by FT-IR (Figure 1) and previously reported by XPS analysis.[38]

From Figure 8(b), it is clear that no As peaks were recorded in the EDX spectrum, probably because the amount of this element was below the detection limit of the equipment. The silicon signal in Figure 8(b) is probably due to accidental contamination from silicon oxide (for example a sand particle).

2.5. Mechanism of As(III) Photocatalytic Oxidation

Oxidative heterogeneous photocatalysis has been shown as a good alternative for As(III) oxidation. Heterogeneous photocatalysis is a very well-known process, valuable for purification and remediation of water and air. Several excellent papers review the subject, with different approaches.[39–40] As very well established, after irradiation of a semiconductor (SC) with light of energy enough for excitation, electrons are promoted from the valence band (VB) to the conduction band (CB), and holes remain in the VB. From a thermodynamic point of view, an acceptor A can be photocatalytically reduced by CB electrons (e_{CB}^-) if its redox potential is more positive than that of the e_{CB}^-, and a donor D can be oxidized by VB holes (h_{VB}^+) if its redox potential is less positive than that of the h_{VB}^+.

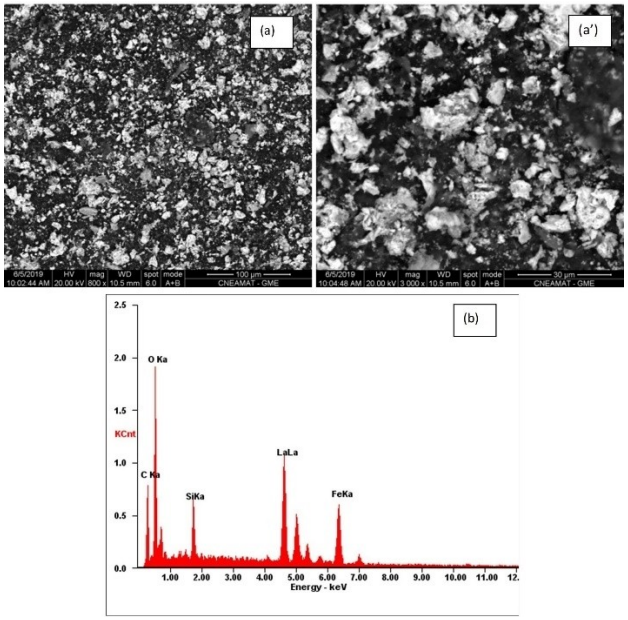

Figure 8. SEM images (a) and (a') and EDX analysis (b) of the $LaFeO_3$ powder after reaction with As.

As said, TiO_2 is the most widely investigated semiconductor because of its good chemical and environmental stability, photocatalytic efficiency, favorable chemical properties and low cost.[5–7] Mechanisms for As(III) photocatalytic oxidation were reported generally over TiO_2 in studies that spanned concentrations from the micro- to the millimolar range, showing in every case very fast oxidation in 10–100 min. Our previous reviews describe the latest advances.[6,41–44] However, other semiconductors can be used, some of them more suitable for irradiation under visible light. The photocatalytic activity of a SC depends on several factors such as the surface area, crystallinity and nature of the surface of the material, pH, etc. Since photocatalytic reactions occur at the surface of the SC, the surface area and affinities of reactants are considered among the most important factors determining the photocatalytic activity, together with the survival of photogenerated charge-carriers before recombination.[39,45] The redox level of the couples related to the levels of the CB and VB can be considered as the most important parameter to predict the feasibility of photocatalytic transformations. We have postulated that the photocatalytic transformation of metal and metalloid ions occurs through successive one-electron transfer steps, if they are thermodynamically allowed. This fact is generally not taken into account by most photocatalytic researchers, despite multielectronic processes are not feasible at the low light intensities usually employed in photocatalysis, and no proof of these processes in semiconductor photocatalytic systems has been reported.[41,42,46] In this way, an inorganic chemical species M (M represents here a metal or a metalloid species, e.g. As(III) in the photocatalytic system can be oxidized by h_{VB}^+ or $HO^\bullet$ (Eq. (1)), provided it has a suitable redox potential for making such reactions thermodynamically possible:

$$M^{n+} + h_{VB}^+ / HO^\bullet \rightarrow M^{(n+1)+} \quad (1)$$

For the present $LaFeO_3$ sample, the value of the bandgap has been determined to be 2.48 eV. Natali Sora et al. found that the position of the quasi-Fermi level of electrons for calcined $LaFeO_3$ photocatalysts is −0.63 V with respect to the Ag/AgCl reference electrode at pH 7; this value can be converted to −0.43 against SHE (all the following reduction potentials in the paper will be referred to the standard hydrogen electrode (SHE).[14] Therefore, the edges of CB and VB at pH 7 have been calculated to be −0.63 and +2.05 V, respectively. The processes can be depicted by the following simplified equations:

$$SC + h\nu \rightarrow e_{CB}^- + h_{VB}^+ \quad (2)$$

$$e_{CB}^- + A \rightarrow A^{\bullet -} \quad (3)$$

$$h_{VB}^+ + D \rightarrow D^{\bullet +} \quad (4)$$

In particular, water or hydroxyl groups adsorbed or present on the SC surface can be oxidized by h_{VB}^{+}, generating $HO^{\bullet}$ (Eq. (5)), while adsorbed O_2 can be reduced by e_{CB}^{-}, generating superoxide radicals, $O_2^{\bullet-}$ (Eq. (6)), in a thermodynamically feasible but rather slow electron transfer reaction.[47,48]. These cathodic pathways are additional sources of $HO^{\bullet}$ (Eq. (9)):

$$h_{VB} + {+}H_2O_{ads}/OH_{surf}^{\bullet-} \rightarrow HO^{\bullet}\ (+H^{+}) \quad (5)$$

$$O_{2ads} + e_{CB}^{-}\ (+H^{+}) \rightarrow O_2^{\bullet-}\ (HO_2^{\bullet}) \quad (6)$$

$$O_2^{\bullet-} + H_2O \rightarrow HO_2^{\bullet} + OH^{-} \quad (7)$$

$$2HO_2^{\bullet} \rightarrow O_2 + H_2O_2 \quad (8)$$

$$H_2O_2 + e_{CB}^{-}\ (O_2^{\bullet-}) \rightarrow\ HO^{-} + HO^{\bullet}\ (+O_2) \quad (9)$$

Therefore, oxidation of As(III) to As(V) can take place by h_{VB}^{+} or $HO^{\bullet}$ attack, although other reactive oxygen species, ROS, formed in the system, such as $O_2^{\bullet-}$, $HO_2^{\bullet}$, H_2O_2, HO_2^{-}, etc., might also carry out the oxidation.[39]

To explain the mechanism of As(III) oxidation, monoelectronic steps with formation of As(IV) that could involve either the reaction with $HO^{\bullet}$ (Eq. (10)), with VB holes (Eq. (11)), or with $O_2^{\bullet-}$ (Eq. (12)) have been suggested:

$$As(III) + HO_{ads}^{\bullet}\ (\text{or } HO_{free}^{\bullet}) \rightarrow As(IV) + OH^{-} \quad (10)$$

$$As(III) + h_{VB}^{+} \rightarrow As(IV) \quad (11)$$

$$As(III) + HO_2^{\bullet}/O_2^{\bullet-} \rightarrow As(IV) + HO_2^{-}/O_2 \quad (12)$$

At pH >6, the predominant As(IV) species are $HAsO_3^{-}$ and AsO_3.[2–49] The standard reduction potential of the As(IV)/As(III) couple has been reported to be around +2.4 V,[49] i.e., ca. 2.0 V at pH 7. Therefore, formation of As(IV) at that pH by attack of holes (E = 2.05 V) is rather thermodynamically possible under the working conditions. Attack by $HO^{\bullet}$ (1.8 V)[50] or $HO_2^{\bullet}/O_2^{\bullet-}$ cannot carry out the oxidation of As(III) to As(IV) at pH 7, because the reduction potential of the $HO^{\bullet}$/HO- is 1.8 V,[50] and that of the $O_2^{\bullet-}/H_2O_2$ couple is around 1.3 V at this pH.[51–52] A schematic representation of mechanisms of As(III) photocatalytic oxidation is shown in Scheme 1.

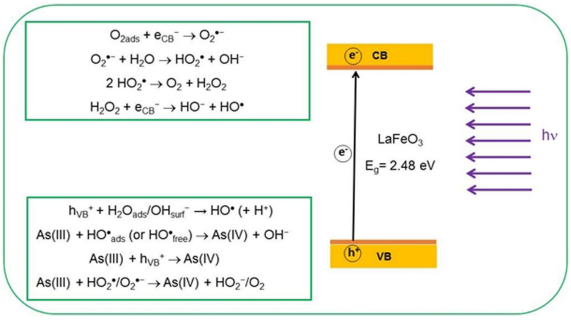

Scheme 1. Representation of mechanisms of As(III) photocatalytic oxidation.

Regardless of the first oxidation step, As(IV) goes further easily to As(V), the stable form. As(IV) reacts with O_2, almost at a diffusion-limited rate,[53] and it is also able to react with other ROS because the reduction potential of As(IV) to As(V) is +1.99 V at pH 7.[49]

$$As(IV) \xrightarrow{O_2/O_2^{\bullet-}/h_{VB}^{+}/HO^{\bullet}} As(V) \quad (13)$$

The mechanism of photocatalytic oxidation of As(III) has been a matter of discussion for many years, the controversy being centered on determining the major oxidant in the system, either $O_2^{\bullet-}$ $HO^{\bullet}$ or h_{VB}^{+}.[48,53] However, whatever the oxidant is, it is not possible to deny the efficiency of the heterogeneous photocatalytic process to transform As(III) into As(V). Dissolved As(V) present in the system can be easily removed by the addition of a suitable adsorbent (mainly containing iron), which will retain the remaining As in solution. The same $LaFeO_3$ can do this action.

3. Conclusions

This study investigates the performance of a perovskite-type lanthanum ferrite to remove arsenic from water, in the dark and under UV-C (254 nm) irradiation, and two different photocatalyst doses. $LaFeO_3$ was prepared by citrate auto-combustion of dry gel obtained from a solution of the corresponding nitrates poured into citric acid solution and characterized. The XRD results confirmed that a monophasic orthorhombic perovskite $LaFeO_3$ powder was obtained, and FT-IR analysis revealed the presence of carbonate species on the surface of the perovskite. The specific surface area was 13 $m^2 g^{-1}$ and the crystallite size was 43 nm after calcining at 600 °C. SEM images showed clusters of particles in the range 100–400 μm and smaller aggregates below 10 μm. DRS analysis reveals a direct bandgap transition of 2.48 eV. Although $LaFeO_3$ has already been tested in heterogeneous photocatalysis for water treatment, it is now for the first time utilized to oxidize soluble As(III) into As(V). Complete removal of As(III) was observed within 60 min of irradiation at 254 nm, due to As(III) photooxidation to As(V). To explain the mechanism of As(III) oxidation, monoelectronic steps with formation of As(IV) have been suggested. As(IV) reacts with O_2, almost at a diffusion-limited rate, and it is also able to react with other ROS because the reduction potential of As(IV) to As(V) is +1.99 V at pH 7. A future work will test the efficiency of this sample for irradiation under visible light.

Experimental Section

Catalyst Synthesis

$LaFeO_3$ nanopowder (LF) was prepared by citrate auto-combustion of dry gel obtained from a solution of the corresponding nitrates poured into citric acid solution, as described in our previous work.[33] Analytical grade La_2O_3, $Fe(NO_3)_3 \cdot 9H_2O$, citric acid, nitric acid and aqueous NH_3 (Sigma-Aldrich) were used as the starting

materials. Briefly, a specific amount of dried La_2O_3 was dissolved in a nitric acid solution (65% m/m) to prepare $La(NO_3)_3 \cdot 6H_2O$. The resulting powder was calcined at 600 °C for 3 h in air. Iron nitrate was dissolved in water (0.1 M) by stirring on a hotplate, and then the solution was poured in citric acid solution, with the molar ratio of iron to citric acid being set at 1:1. Aqueous NH_3 was added slowly until pH 6.8, and the solution turned transparent. The solution was then dehydrated until a brown/orange $LaFeO_3$ gel formed. The dry gel was heated in air to 250 °C to start ignition. The resulting lightweight powder was calcined at 600 °C for 3 h to remove any organic residue and an ochre $LaFeO_3$ powder was obtained after calcination.

Fresh Catalyst characterization

XRD pattern was collected at room temperature using a Bruker D8 diffractometer θ-2θ arrangement ($Cu_{K\alpha}$ radiation). The measuring conditions were within the 5–70° 2θ range, with steps of 0.02° 2θ with a scan rate of 1.2° min^{-1}. Phase analysis was performed with the DIFFRAC.EVA software (Bruker AXS) using the PDF 2019 Database. The crystallite size was calculated using the Scherrer equation. The SSA of the powder was determined with a Sorptomatic 1990 instrument by Thermo Fisher Scientific. The FTIR spectra were collected in a Bruker Tensor 27 spectrophotometer accumulating 50 scans at a resolution of 4 cm^{-1} for the measurements in the transmittance mode. The UV-Vis diffuse reflectance spectroscopy (DRS) spectrum was recorded in the 200–800 nm range by using a Jasco V-650 spectrophotometer equipped with an integrating sphere for solid samples, with $BaSO_4$ as the reference sample. SEM analysis was performed using a FEI Company instrument, model Quanta 200, with field emission operated at 25 kV. The SEM images were recorded at different magnifications at a 25 kV operating voltage (field emission), at an acceleration voltage of 20 kV. The nanoparticles were analyzed with an EDS detector, Oxford Instruments. The samples ($LaFeO_3$ powder and the solids recovered at the end of each experiment of As removal attached to the filter) were first affixed onto carbon adhesive tapes supported on metallic disks and then covered with a thin, gold, electrically conductive film.

Arsenic removal tests

For experiments in the dark and under irradiation, a batch system was used, constituted by a cylindrical Pyrex glass (reservoir) with a jacket for water circulation and thermostatization (reservoir), 40 mm long, 35 mm external diameter and 400 mL total volume, provided with a vertical Decalab paddle stirrer. For experiments under UV-C irradiation, the same setup was used, arranging a UV-C lamp (low pressure mercury, $\lambda max = 254$ nm, G15T8, output 15 W, OSRAM, PURITEC model) at the central axis of a totally sealed tube (see setup in the Supporting information file). The irradiated volume inside the tube containing the lamp was 100 mL. The photon flux per unit volume ($q^0_{n,p}/V$) incident in the suspension for the UV-C lamp was 24.5 μeinstein $s^{-1} L^{-1}$, measured by ferrioxalate actinometry under the same conditions as those of the photocatalytic experiments. All the experiments, in the dark and under irradiation were carried out at 25 °C, controlled by a thermocirculator (PolyScience).

Experiments of As(V) and As(III) removal (both 1 mg L^{-1}) with $LaFeO_3$ were performed in the dark with the reactor open to the air. For experiments with As(V), sodium dibasic arsenate heptahydrate ($Na2HAsO_4 \cdot 7H_2O$, Baker) was used, while for As(III), sodium metaarsenite (Baker) was used. For experiments with As(V) in the dark, a suspension (200 mL) was prepared using 1.49 mg of $LaFeO_3$ at an As:Fe molar ratio (MR) = 1:10) and 14.9 mg for MR = 1:100 (pH 7). For experiments of As(III) in the dark, a suspension (400 mL) was prepared using 8.96 mg of LaFeO3 for MR = 1:30 and 29.8 mg for MR = 1:100 (pH 6–7). All solutions in this work have been prepared with Milli-Q water. The suspensions were put in the cylindrical reservoir, with the paddle stirrer running during all the experiment. For the experiments under irradiation, a peristaltic pump was used for the recirculation (1.5 L min^{-1}) of the suspension from the reservoir through the tube; the lamp was started immediately after the addition of the suspension. A small pH variation was observed at the end of all the experiments, while keeping pH to vary freely.

In all cases, periodical samples (3 mL) were taken, filtered through 0.2 μm cellulose acetate filters (Sartorius) and As(III), As(V) and As_T in solution were measured by a modification of the arsenomolybdate or molybdenum blue method (detection limit (DL): 0.01 mg L^{-1}).[34,35] The molybdenum blue method measures As(V). Two solutions are used: 1. 10% w v-1 ascorbic acid (Anedra) solution prepared freshly before use; 2. reagent solution "A": 0.13 g L^{-1} potassium antimonyl tartrate (Baker) and 5.8 g L^{-1} ammonium molybdate (Stanton). Both solutions were mixed with 5 M H_2SO_4 (Anedra) in a 500 mL beaker. This reagent is stable for two months stored in an opaque bottle. A volume of sample containing As(V) was placed in a 25 mL flask. Then 400 μL of fresh 10% m V^{-1} ascorbic acid solution was added, together with 800 μL of solution A, the solution was made up to the mark with Milli-Q water and allowed to react in a water bath at 37 °C for 30 min. Then, the sample was allowed to cool to room temperature for 30 min and the absorbance at $\lambda = 868$ nm was finally measured using a UV/VIS HP8453A spectrophotometer in a 5 cm cell. For AsT determination, 400 μL of 3 mM potassium permanganate (Riedel de Haën) solution was added to each sample, to guarantee the total oxidation of As(III) to As(V), left to react for 5 min and then the determination of As(V) was carried out analogously. By difference of AsT and As(V), the concentration of As(III) was determined.

Solids from selected photocatalytic experiments obtained after complete As removal were separated by filtration, dried for 24 h at 50 °C and analysed by SEM-EDS.

Acknowledgements

This work was supported by Agencia Nacional de Promoción Científica y Tecnológica (ANPCyT) from Argentina under PICT-2015-0208 and the National Interuniversity Consortium of Materials Science and Technology (INSTM) from Italy. Thanks to Prof. L. Malavasi for the SSA determination.

Conflict of Interest

The authors declare no conflict of interest.

Keywords: arsenic removal · lanthanum ferrite · photocatalysis perovskite-type species · UV-C irradiation

[1] R. Singh, S. Singh, P. Parihar, V. P. Singh, S. M. Prasad, *Ecotoxicol. Environ. Saf.* **2015**, *112*, 247–70.
[2] WHO. Arsenic in Drinking Water; W. H. Organisation Ed.; WHO: Geneva, Switzerland, **2011**.
[3] N. R. Nicomel, K. Leus, K. Folens, P. Van der Voort, G. Du Laing, *Int. J. Environ. Res. Public Health* **2016**, *13*, 62–85.

[4] W. Choi, J. Yeo, J. Ryu, T. Tachikawa, T. Majima, *Environ. Sci. Technol.* **2010**, *44*, 9099–9104.
[5] X. H. Guan, J. S. Du, X. G. Meng, Y. K. Sun, B. Sun, Q. H. Hu, *J. Hazard. Mater.* **2012**, *215*, 1–16.
[6] M. I. Litter, *Curr. Opin. Green Sustain. Chem.* **2017**, *6*, 150–158.
[7] R. Molinari, P. Argurio, *Water Res.* **2017**, *109*, 327–336.
[8] P. K. Dutta, A. K. Ray, V. K. Sharma, F. J. Millero, *J. Colloid Interface Sci.* **2004**, *278*, 270–275.
[9] M. Li, Z. Hong, Y. N. Fang, F. Q. Huang, *Mater. Res. Bull.* **2008**, *43*, 2179–2186.
[10] R. Abazari, S. Sanati, L. A. Saghatforoush, *Mater. Sci. Semicond. Process.* **2014**, *25*, 301–306.
[11] A. Marcucci, F. Zurlo, I. N. Sora, E. Placidi, S. Casciardi, S. Licoccia, E. Di Bartolomeo, *J. Mater. Chem. A* **2019**, *7*, 5344–5352.
[12] J. M. Tulliani, M. M. Natile, L. Tortora, I. N. Sora, *Chem. Eng. Trans.* **2015**, *43*, 1807–1812.
[13] R. Spinicci, A. Tofanari, M. Faticanti, I. Pettiti, P. Porta, *J. Mol. Catal. A* **2001**, *176*, 247–252.
[14] I. N. Sora, F. Fontana, R. Passalacqua, C. Ampelli, S. Perathoner, G. Centi, F. Parrino, L. Palmisano, *Electrochim. Acta* **2013**, *109*, 710–715.
[15] V. M. Gaikwad, P. Uikey, S. A. Acharya, *AIP Conf. Proc.* **2015**, *1665*, 140046.
[16] M. Ismael, M. Wark, *Catalysts* **2019**, *9*, 342.
[17] J. Yang, H. Q. Zhong, M. Li, L. Z. Zhang, Y. M. Zhang, *React. Kinet. Catal. Lett.* **2009**, *97*, 269–274.
[18] P. Kanhere, Z. Chen, *Molecules* **2014**, *19*, 19995–20022.
[19] S. D. Li, L. Q. Jing, W. Fu, L. B. Yang, B. F. Xin, H. G. Fu, *Mater. Res. Bull.* **2007**, *42*, 203–212.
[20] K. M. Parida, K. H. Reddy, S. Martha, D. P. Das, N. Biswal, *Int. J. Hydrogen Energy* **2010**, *35*, 12161–12168.
[21] G. Iervolino, V. Vaiano, D. Sannino, L. Rizzo, P. Ciambelli, *In International Conference on Nanotechnology Based Innovative Applications for the Environment*, Vol 47 (Eds. A. Chianese, L. Di Palma, E. Petrucci, M. Stoller) **2016**, pp. 283–288.
[22] N. Turkten, I. N. Sora, A. Tomruk, M. Bekbolet, *Catalysts* **2018**, *8*, 630.
[23] H. J. Su, L. Q. Jing, K. Y. Shi, C. H. Yao, H. G. Fu, *J. Nanopart. Res.* **2010**, *12*, 967–974.
[24] K. X. Wang, H. L. Niu, J. S. Chen, J. M. Song, C. J. Mao, S. Y. Zhang, Y. H. Gao, *Appl. Surf. Sci.* **2017**, *404*, 138–145.
[25] I. N. Sora, D. Fumagalli, *Environ. Sci. Pollut. Res. Int.* **2017**, *24*, 12556–12561.
[26] S. N. Tijare, M. V. Joshi, P. S. Padole, P. A. Mangrulkar, S. S. Rayalu, N. K. Labhsetwar, *Int. J. Hydrogen Energy* **2012**, *37*, 10451–10456.
[27] G. P. Wheeler, V. U. Baltazar, T. J. Smart, A. Radmilovic, Y. Ping, K. S. Choi, *Chem. Mater.* **2019**, *31*, 5890–5899.
[28] R. Pelosato, V. Carrara, I. Natali Sora, *Chem. Eng. Trans.* **2019**, *73*, 181–186.
[29] S. H. Dong, K. J. Xu, G. S. Tian, *J. Mater. Sci.* **2009**, *44*, 2548–2552.
[30] Q. Liang, J. Jin, C. H. Liu, S. Xu, Z. Y. Li, *J. Alloys Compd.* **2017**, *709*, 542–548.
[31] Q. Peng, J. Wang, Z. J. Feng, C. Du, Y. W. Wen, B. Shan, R. Chen, *J. Phys. Chem. C* **2017**, *121*, 12991–12998.
[32] Y. C. Ye, H. Yang, R. S. Li, X. X. Wang, *J. Sol-Gel Sci. Technol.* **2017**, *82*, 509–518.
[33] T. Caronna, F. Fontana, I. Natali Sora, R. Pelosato, *Mater. Chem. Phys.* **2009**, *116*, 645–648.
[34] V. Lenoble, V. Deluchat, B. Serpaud, J. C. Bollinger, *Talanta* **2003**, *61*, 267–276.
[35] I. K. Levy, M. Mizrahi, G. Ruano, G. Zampieri, F. G. Requejo, M. I. Litter, *Environ. Sci. Technol.* **2012**, *46*, 2299–2308.
[36] P. Kubelka, *J. Opt. Soc. Am.* **1954**, *44*, 330–335.
[37] K. Rusevova, R. Köferstein, M. Rosell, H. H. Richnow, F–D Kopinke, A. Georgi, *Chem. Eng. J.* **2014**, *239*, 322–331.
[38] F. Parrino, E. García-López, G. Marcì, L. Palmisano, V. Felice, I. Natali Sora, L. Armelao, *J. Alloys Compd.* **2016**, *682*, 686–694.
[39] M. R. Hoffmann, S. T. Martin, W. Y. Choi, D. W. Bahnemann, *Chem. Rev.* **1995**, *95*, 69–96.
[40] K. Nakata, A. Fujishima, *J. Photochem. Photobiol.* **2012**, *13*, 169–189.
[41] M. I. Litter, *Adv. Chem. Eng.* **2009**, *36*, 37–67.
[42] M. I. Litter, N. Quici, in: *Nanomaterials for Environmental Protection*, Chapter 9. (Editors: B. I. Kharisov, O. V. Kharissova, H. V. Rasika Dias) John Wiley & Sons, Hoboken, **2014**, pp. 145–167.
[43] M. I. Litter, *Pure Appl. Chem.* **2015**, *87*, 557–567.
[44] M. I. Litter, N. Quici, J. M. Meichtry, A. M. Senn, in: *Photocatalysis: Applications*, (Editors: D. D. Dionysiou, G. Li Puma, J. Ye, J. Schneider, D. Bahnemann), Royal Society, Chap. 2, **2016**, pp. 35–71.
[45] H. Kominami, S. Murakami, J. Kato, Y. Kera, B. Ohtani, *J. Phys. Chem. B* **2002**, *106*, 10501–10507.
[46] P. V. Kamat, *J. Phys. Chem. Lett.* **2012**, *3*, 663–672.
[47] H. Gerischer, A. Heller, *J. Phys. Chem.* **1991**, *95*, 5261–5267.
[48] J. Ryu, W. Y. Choi, *Environ. Sci. Technol.* **2006**, *40*, 7034–7039.
[49] U. K. Kläning, B. H. J. Bielski, K. Sehested, *Inorg. Chem.* **1989**, *28*, 2717–2724.
[50] W. H. Koppenol, *Nature* **1976**, *262*, 420–421.
[51] Y. A. Ilan, G. Czapski, D. Meisel, *Biochim. Biophys. Acta* **1976**, *430*, 209–224.
[52] P. Wardman, *J. Phys. Chem. Ref. Data* **1989**, *18*, 1637–1755.
[53] H. Fei, W. Leng, X. Li, X. Cheng, Y. Xu, J. Zhang, C. Cao, *Environ. Sci. Technol.* **2011**, *45*, 4532–4539.

Manuscript received: March 13, 2021
Revised manuscript received: July 9, 2021